ELSEVIER

Coordination Chemistry Reviews
149 (1996) 281–309

COORDINATION CHEMISTRY REVIEWS

Defining speciation profiles of Al^{3+} complexed with small organic ligands: the Al^{3+}–heidi system

Peter A. Jordan [a], Nigel J. Clayden [a], Sarah L. Heath [a], Geoffrey R. Moore [a,*], Annie K. Powell [a], Andrea Tapparo [b]

[a] *Centre for Metalloprotein Spectroscopy and Biology, School of Chemical Sciences, University of East Anglia, Norwich, Norfolk NR4 7TJ UK*

[b] *Dipartimento di Chimica Inorganica, Metallorganica ed Analitica, Università degli Studi di Padova, Padova, Italy*

Received 15 February 1995

Contents

* Corresponding author.

0010-8545/96/$32.00 © 1996 Elsevier Science S.A. All rights reserved
SSDI 0010-8545(95)01177-3

Abstract

One of the outstanding chemical problems associated with the biological importance of aluminium is the definition of speciation profiles for Al^{3+} in biological fluids. By speciation profiles is meant the distribution of Al^{3+} among its different complexes, and their structures, stability constants and rates of formation and breakdown. As is often the case with metal speciation, it is the complexes formed with small ligands that present most experimental difficulties. A procedure is described for characterizing speciation profiles for Al^{3+} complexed to small organic ligands, the approach being illustrated with the Al^{3+}–heidi system. It is shown that comparative solution NMR and potentiometric studies are in reasonable agreement concerning the number and identity of the major Al^{3+}–heidi components present in a solution, but the exact structures of the major species are uncertain in some cases. The main approach to determining such structures involves X-ray diffraction studies of crystals obtained from the given solutions, but whether the crystalline forms represent a thermodynamically preferred species in solution is not always clear. Bridging the gap between solid and solution structures is shown to be problematic, even with the comparative vibrational spectroscopies and solid-state NMR.

Keywords: Speciation; Bioavailability, Heidi, ^{1}H, ^{13}C, ^{27}Al NMR

1. Introduction

Although aluminium is the most abundant metal in the Earth's crust, it was, until the recent intervention of man, largely unavailable to biological systems and thus does not have any important roles in biology [1]. In fact, the toxicity of aluminium to a variety of organisms is well established, ranging from dialysis dementia in patients with kidney disease undergoing dialysis treatment to "Waldsterben", suffered by trees in forests subject to acid rain, and the poisoning of fish in lakes (Refs. [1–7] and references cited therein). In many cases, the biological effect of such toxicity is well documented and includes enzyme inhibition, nucleotide destruction and mineral formation. However, this only represents the end product of a complex chain of reactions that are largely unknown, and often undetected within a biological system by nutritional, biochemical and medical studies. Since the effects of the toxic metal ion are a function of its bioavailability, it is important to determine the constraints involved in the stages from absorption to the site(s) of action.

Aluminium is probably able to enter organisms by utilizing iron uptake pathways [1–3,8]. Because aluminium has, until recently, not been bioavailable, it is possible that organisms have not developed the ability to discriminate between this toxic metal ion and the iron(III) ion. Both ions have similar chemistries and ionic sizes [although Al(III) is ca. 10% smaller in radius] with one of the major features being their pronounced and extensive hydrolysis reactions [9]. This latter is a key feature in determining the bioavailability of iron, and a variety of methods for controlling iron(III) hydrolysis, and thereby the levels of iron in cells, have evolved. For example, the transport of iron(III) within mammals is accomplished by chelating iron(III) as a mononuclear centre (of which there are two) within the protein transferrin [10–14],

whereas excess iron is stored in the form of a hydrolysed giant polyiron(III) oxyhydroxide cluster corresponding to a fragment of mineralised iron(III) held within the protein ferritin [12–16]. It appears that the aluminium(III) ion can be assimilated and transported using the iron pathways, but not stored in the same way, and it is at this point that the toxic effects of aluminium manifest themselves by disrupting the biochemistries of other metal ions such as magnesium(II), calcium(II), and possibly also phosphate biochemistry [1–3,8,17].

Our programme of research into the background to the toxic effects of aluminium have so far concentrated on developing methods for following the solution-state speciation of aluminium and comparing the hydrolytic behaviour of aluminium in the presence of biologically relevant ligands with that of iron(III) [18,19]. This recognizes the fact that the hydrolysis of these metal ions is modified by the presence of a variety of potential ligands ranging from organic and inorganic species such as humic acid, phosphates and chloride in natural waters through to ligands derived from the diet (citrate, lactate, amino acids, etc.) in the gastro-intestinal tract on to protein amino acid side-chains at metal sites in proteins.

The procedure we have adopted for characterizing speciation profiles for Al^{3+} complexed to small organic ligands employs a combination of solid- and solution-state physical methods as summarized in Fig. 1. Of the methods listed, only X-ray diffraction can give molecular structures to high resolution. However, there are two problems with the application of this method to studies of speciation. First, single crystals are not always obtained under the biologically relevant conditions, and second, the solid species may not be representative of the major species in solution. However, by employing comparable solution-state studies it is often possible to predict the dominant species present in solution. In this paper we illustrate this approach using the Al^{3+}–heidi system as a case history. We begin, however, by describing the techniques listed in Fig. 1, and their applications and limitations.

2. Techniques employed

Throughout the discussion of the techniques employed to define speciation profiles, it should be borne in mind that different solution-state studies are often performed under different conditions. This is partly because different laboratories use different reagents and partly because different techniques have different solution requirements. For example, some of the potentiometric studies cited in this review have been carried out at widely different dilutions, and for a hydrolytic ion such as Al^{3+} this is likely to have a dramatic effect. Further factors which are often ignored when comparing solution state measurements are the following:

(a) The ionic strength of the solution. In potentiometric studies this is held constant by the addition of salts. However, these in turn can affect the solubilities of species via, for example, common ion effects.
(b) The source of the Al^{3+}. Speciation is likely to be different with Cl^-, NO_3^- and SO_4^{2-} ions present in solution.
(c) The acid or base used to adjust pH. Local pH gradients are known to be capable

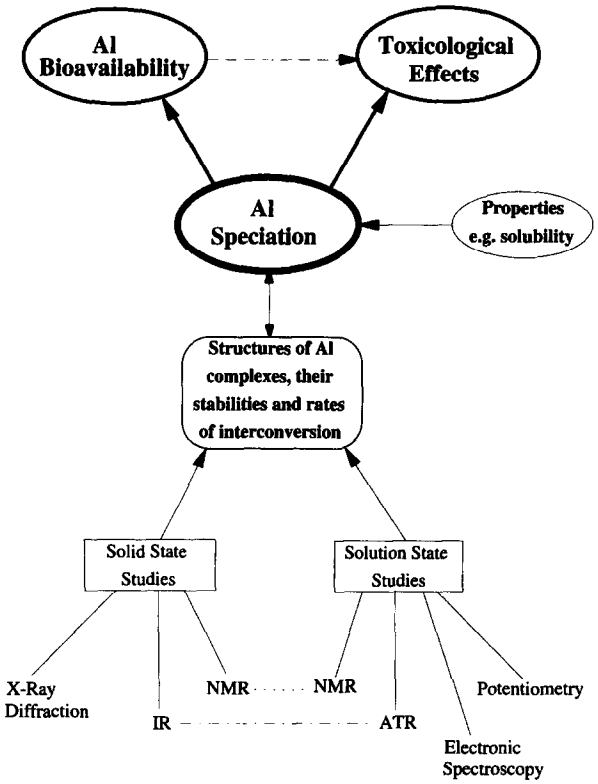

Fig. 1. Illustration of the range of techniques available for determining the speciation of Al^{3+} under a given set of conditions. Moving on from the speciation profile to determining bioavailability and toxicological effects, which are the biological objectives, requires knowledge of particular properties of the aluminium species, such as their solubilities in different types of solvents. Such properties, which are rarely known, are not considered in this article.

of influencing the degree of aggregation observed in the condensation reactions associated with hydrolysis. A strong base, for example, will induce a steeper pH gradient [20].

As yet, it has not been possible to maintain constant conditions for all experimental procedures, but this is a goal which we are striving to achieve. At the very least these variables need to be taken into account when discussing comparative solution-state techniques.

2.1. Potentiometric pH titrations

The determination of stability constants by potentiometric pH titrations is a powerful method for defining the identity and distribution of metal–ligand complexes, and hence investigating speciation in aqueous systems. Recent advances have greatly improved the reliability of such studies and there are a number of texts available

that describe the background theory and experimental details [21,22]. A key breakthrough has been the development of computational methods for data processing which have greatly increased the speed and accuracy with which stability constants can be determined. In addition, this has increased the range and complexity of possible investigations with multidentate ligands and multicomponent systems now being regularly studied. The application of potentiometry to aluminium–ligand systems is not straightforward, mainly because of the presence of numerous hydrolysis equilibria and the slow kinetics which characterize them [23].

Potentiometry is a common technique for determining stability constants because of the simplicity of the experimental apparatus and the ease with which it can be automated. Although ion-specific electrodes can be used to measure specific ion concentrations, it is usually sufficient to use accurate glass electrodes to measure the hydrogen ion concentration. Such an approach works well for aluminium as direct observations of the metal ion in solution are not required. However, to avoid errors in the final analysis, it is important to account for the slow kinetics of aluminium–ligand interactions to ensure that equilibrium measurements are made.

Standard experimental procedures involve the incremental addition of a base to a characterized acid solution of the ligand in the absence and presence of known metal ion concentrations. Data analysis is a fairly automated procedure with basic computer programs available for the calibration of the initial system and more complicated programs employed to evaluate the metal ligand interaction [24]. These programs are based on a minimization procedure that uses algorithms to refine an initial trial solution to convergence. Care must be taken to rationalise the results as it is possible for a wrong solution to converge. Fortunately, most programs also perform an error analysis on the results so mistakes should be minimized. A final pitfall to avoid is over-interpretation of the results, often due to a confusion between macroscopic and microscopic stability constants (see Fig. 2). This highlights one of the major drawbacks of stability constants, namely that although the number of species in solution and their charges may be determined, it is normally not possible to define structural details.

There have been many potentiometric investigations reported on the interaction of Al(III) with biologically relevant ligands, such as citrate, and these studies highlight some of the strengths and weaknesses of this technique, with apparent disagreement between much of the published work. However, a close investigation reveals that the results obtained are generally consistent, although they are crucially dependent on experimental conditions, with concentration and equilibrium times affecting the nature of the species formed [24,26–28]. Therefore, the parallel use of other techniques is useful to allow the solution speciation to be adequately characterized. An example of the kind of speciation profile obtained from considering hydrolytic species of Al^{3+} is given in Fig. 3. The figure shows first that there is a variety of polymeric and monomeric species that can be formed and second that there is a strong concentration dependence to the speciation.

There have been a number of computer models based on known stability constants developed to simulate aluminium speciation in environments such as soil, rivers and blood plasma, and in the assessment of potential *in vivo* aluminium chelators

$$Fe^{3+} + Tf + HCO_3^- \overset{K_1}{\rightleftharpoons} CO_3^{2-}\text{-}Fe^{3+}\text{-}Tf + 3H^+ \quad (1)$$

$$Fe^{3+} + CO_3^{2-}\text{-}Fe^{3+}\text{-}Tf + HCO_3^- \overset{K_2}{\rightleftharpoons} (CO_3^{2-}\text{-}Fe^{3+})_2\text{-}Tf + 3H^+ \quad (2)$$

$$K_1 = \frac{[CO_3^{2-}\text{-}Fe^{3+}\text{-}Tf][H^+]^3}{[Fe^{3+}]\,[Tf]\,[HCO_3^-]} \quad (3)$$

$$K_2 = \frac{[(CO_3^{2-}\text{-}Fe^{3+})_2\text{-}Tf][H^+]^3}{[Fe^{3+}][CO_3^{2-}\text{-}Fe^{3+}\text{-}Tf][HCO_3^-]} \quad (4)$$

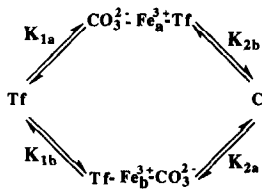

(5)

$$K_1 = K_{1a} + K_{1b} \quad (6)$$

$$1/K_2 = 1/K_{2a} + 1/K_{2b} \quad (7)$$

Fig. 2. Distinction between macroscopic and microscopic constants. The equations describe the well defined case of iron binding to transferrin together with the synergistic anion HCO_3^-–CO_3^{2-} [13,25], but the general thermodynamic scheme will apply to many systems. Eqs. (1) and (2) describe the chemical equilibria for which K_1 and K_2 in Eqs. (3) and (4) are the macroscopic association constants. K_1 and K_2 are related to the intrinsic site constants, or microscopic constants, given in Eq. (5) by the relationships expressed in Eqs. (6) and (7).

[29–31]. Although useful, many of these suffer from the disadvantage that kinetic factors generally cannot be taken into account. Also, the models assume that all biological or environmental equilibrium steps have been identified, and this may not be the case. Nevertheless, this modelling approach is an important development and one that should increase in reliability as further details of the solution speciation of Al^{3+} emerge.

2.2. *X-ray crystallography*

Although a single-crystal X-ray diffraction study can provide precise metrical details of the molecular structure of a complex, as noted above this complex is not necessarily representative of the major species which will exist in solution. For example, it might be one of many different compounds present in solution, or it might not even be important at all in solution, only crystallizing in significant yields by virtue of its insolubility. Another limitation of this method is that it requires

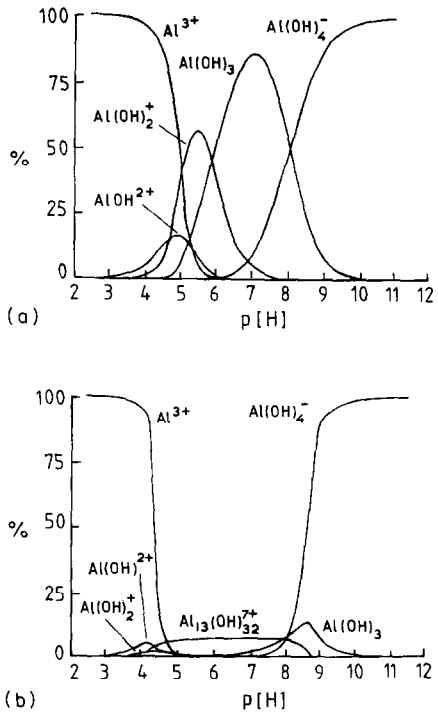

Fig. 3. Solution speciation profile of aqueous aluminium(III) for (a) 1×10^{-6} M $[Al^{3+}]$ and (b) 1×10^{-3} M $[Al^{3+}]$ determined from potentiometric titrations at 25.0 °C and $\mu = 0.1$ M. Adapted from Ref. [26] (see also Ref. [24]).

single crystals and not all complexes can be obtained in a suitable crystalline form. Further details of this method and its application to aluminium-containing complexes can be found in the review by Powell and Heath [32]. In this paper we shall only discuss those crystal structures relevant to the solution speciation we are considering.

2.3. *Nuclear magnetic resonance spectroscopy (NMR)*

2.3.1. *General considerations*

NMR spectroscopy is a powerful method for studying Al^{3+} complexes in the solution and solid states. In addition to ^{1}H and ^{13}C NMR spectra, ^{27}Al NMR spectra can be obtained in a relatively straightforward manner. ^{27}Al is 100% naturally abundant, has a nuclear spin quantum number (I) of 5/2 and is 1170 times more receptive than naturally abundant ^{13}C. However, because it has an $I > 1/2$ it possesses a nuclear quadrupole moment and this produces broad NMR signals for compounds where there is a significant electric field gradient at the ^{27}Al nucleus. In practice, this means almost all cases in which the Al^{3+} ligands are not of the same type or do not form a site of high symmetry [33]. This is illustrated by Fig. 4, which shows the solution-state ^{27}Al NMR spectra of the highly symmetric species $[Al(OH)_4]^-$ and

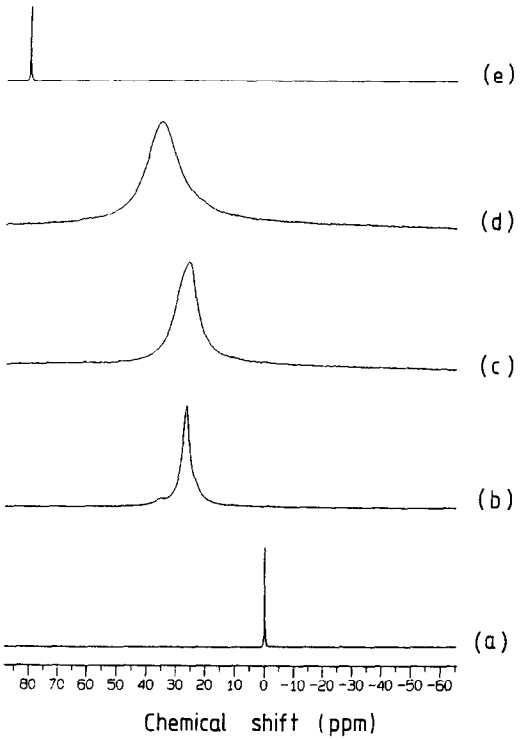

Fig. 4. 104.5 MHz ^{27}Al NMR spectra of (a) $[Al(H_2O)_6]^{3+}$ and (b)–(d) equimolar solutions of Al^{3+} with (b) 1,2-propylenediaminetetraacetic acid (pdta), (c) nitrilotriacetate (nta) and (d) ethylenediaminetretracetate (edta) all at pH 7; (e) $[Al(OH)_4]^-$.

$[Al(H_2O)_6]^{3+}$, and spectra of less symmetric complexes of chelated Al^{3+}. The linewidth variation, which may also be affected by chemical exchange effects, is striking. Both ^1H and ^{13}C have $I=1/2$ and thus do not have nuclear quadrupole moments. However, ^1H and ^{13}C linewidths may be affected by chemical exchange processes.

2.3.2. Solution-state NMR

Solution-state ^1H and ^{13}C NMR spectroscopy has been used extensively to study metal ion complexation with organic ligands. Typically chemical shift perturbations are employed to monitor complex formation. The spectra shown in Fig. 5 for an equimolar solution of Al^{3+} and citrate at pH 7.4 compared with the spectra of citrate alone illustrate both the usefulness of this approach and its limitations. The ^1H spectra are not particularly informative. They do indicate that complex formation has occurred but the complexity of the Al^{3+}–citrate spectrum, with many lines overlapping and forming second-order coupling patterns, means that it gives little information on the number of species formed other than there are multiple species. The ^{13}C spectrum is far more useful, partly because it is better resolved and complica-

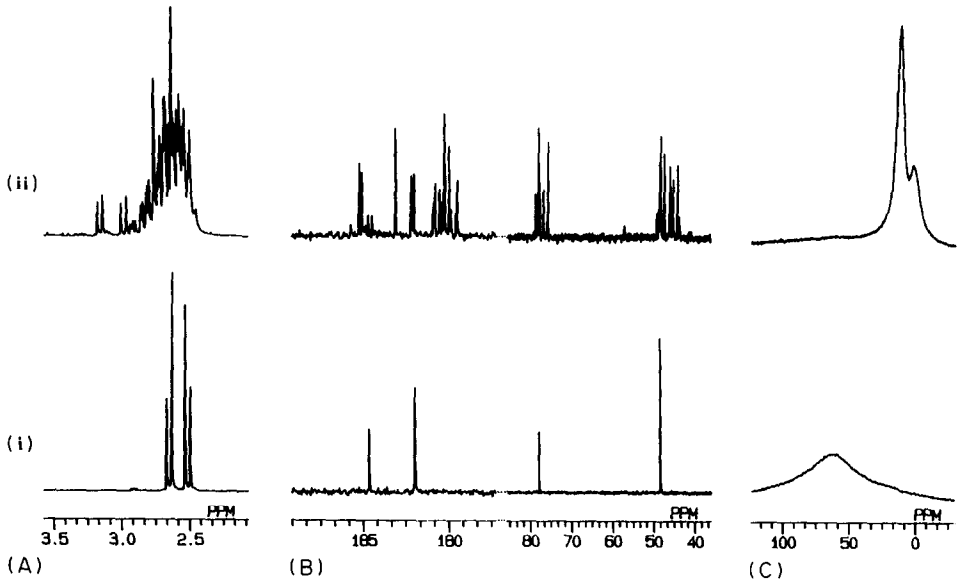

Fig. 5. (A) ^{1}H, (B) $^{13}C-\{^{1}H\}$ and (C) ^{27}Al NMR spectra of 0.1 M citric acid at pH 7.4 in the (i) absence and (ii) presence of 0.1 M Al^{3+}. The broad signal in spectrum (C)(i) is an instrument background signal only seen at high gain. It can be removed by filtering (see Fig. 6).

tions due to spin–spin coupling are not present. It is clear that complex formation has occurred and also that more than one species has been formed. Provided the spectra have been obtained under conditions when the $^{1}H-^{13}C$ nuclear Overhauser enhancement and ^{13}C relaxation time differences have been allowed for, then the relative intensities of different peaks are an indication of the relative amounts of the different citrate species. However, resonance assignment remains a problem, and thus a full analysis of this system has not been possible.

^{27}Al NMR is also not straightforward to interpret, although Fig. 5(c) does show in a direct way that there are at least two types of Al^{3+} in the Al^{3+}–citrate solution. This is further indicated by the ^{27}Al NMR spectra of a dilute, and equimolar, solution of Al^{3+} and citrate at pH 7.4 shown in Fig. 6. The two spectra were measured with different delay times between the observation radiofrequency pulse and data acquisition in order to take account of the relatively large background signal from the spectrometer at ca. 65 ppm which is always present. With a delay of 250 μs this signal is fully relaxed and therefore not recorded. However, the spectrum of citrate-bound Al^{3+} is also affected by this delay and the very broad component at ca. 18 ppm is lost, although the distinctive set of peaks at 13.0 and 0.5 ppm are retained. Comparison of spectrum B with spectrum A reveals that there are at least three signals, indicating that there are at least three Al–citrate complexes present. The relative intensities of the different signals should reflect the relative amounts of the species present but, because the signals have similar chemical shifts and are broad,

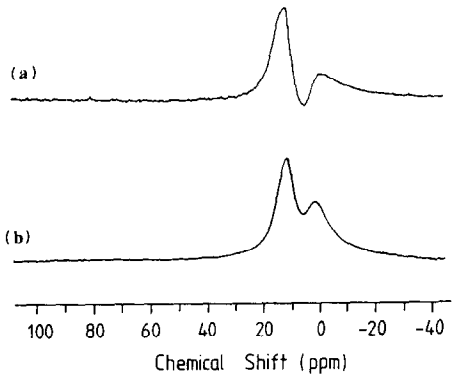

Fig. 6. 104.5 MHz ^{27}Al NMR spectra of 1 mM Al^{3+} and citric acid at pH 7.4. Spectrum (a) was acquired with a delay time of 250 μs between the observation pulse and data acquisition, and spectrum (b) with a delay time of 25 μs. The longer delay time filtered out signals which are rapidly relaxing, and thus are broad.

accurate integration is not possible. Thus, apparently, ^{27}Al NMR gives little additional information to that obtained by ^{13}C NMR. Why, then, is it worth pursuing?

It is worth pursuing for a number of reasons. First, ^{27}Al NMR is far more sensitive than ^{13}C NMR and thus spectra can be acquired much more rapidly. Second, it is not always the case that ^{27}Al NMR and ^{13}C NMR will give identical information regarding the number of species present. This is demonstrated by the inability to detect the aqueous hydrolysis products of Al^{3+} by ^{13}C NMR, and also the sometimes poor ability of ^{27}Al NMR compared with that of ^{13}C NMR to distinguish different complexes of the same ligand. Both cases are demonstrated by the Al^{3+}–malonate system [19]. Third, and most important, ^{27}Al NMR chemical shifts of related complexes differ markedly. This is illustrated by Figs. 4 and 7. The major difference between $[Al(OH)_4]^-$ and $[Al(H_2O)_6]^{3+}$ is due to the difference in coordination

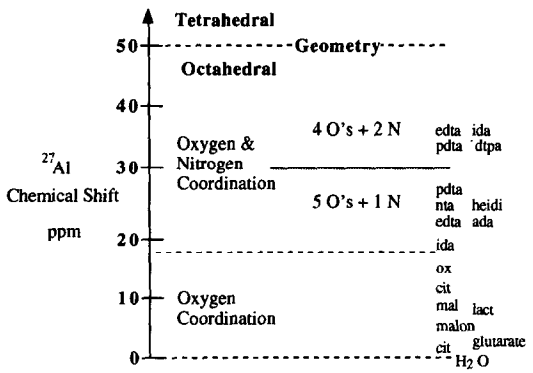

Fig. 7. Chemical shift regions and coordination patterns found in ^{27}Al NMR (adapted from Ref [34]); cit, lact, mal, malon, ox, ada, ida, heidi, dtpa, refer to citrate, lactate, maleate, malonate, oxalate, *N*-(2-acetamido)iminodiacetate, iminodiacetate, *N*-(2-hydroxyethyl)iminodiacetate and diethylenetriaminepentaacetate, respectively; edta, nta and pdta are defined in Fig. 4.

geometry [33,34], octahedral versus tetrahedral, but even within the range associated with octahedral complexes there is a wide variation of chemical shift for apparently similar types of ligands. The origin of this variation is currently under investigation by a number of groups [33–36]. Some of the possibilities are that the chemical shift varies with denticity of the ligand, charge on the ligand or nature of the immediate donor atoms to Al^{3+}. Currently we believe that the identity of the donor atoms is most important.

2.3.3. Solid-state NMR

Solid-state NMR [37] provides an invaluable bridge between solution-state NMR and crystallographic studies. When comparing solution-state NMR data and crystal structures, the problem arises that although we can define a metal ion complex by a set of observed chemical shifts, we cannot show that the complex which crystallizes corresponds to that seen by solution-state NMR. In principle, solid-state NMR can establish a link through a comparison of the NMR data found for the crystal and solution species. Complications arise in this comparison from two sources. First, the greater NMR linewidths seen in the solid state limit the resolution so that fine features in the solution NMR data may be obscured (Fig. 8). Second, specific effects can alter the appearance of the NMR spectrum in the solid state, leading to additional resonances and variations in the chemical shifts. The most obvious of these effects is that the resonance multiplicity may reflect both the crystallographic symmetry and the number of molecules in the unit cell. Allied to this, molecular interactions in the crystal may cause small changes to the chemical shifts from the values seen in solution. The difficulty is not so much that these perturbations occur, but that they are of unpredictable magnitude. Fig. 8 illustrates this for the crystalline $[Al(heidi)(H_2O)_2]_2 \cdot 2H_2O$ dimer (Section 3.2). The ^{27}Al NMR spectrum contains a single isotropic resonance, considerably broader than its corresponding solution-state resonance, with a striking spinning side band pattern, and the ^{13}C spectrum, although clearly similar to the corresponding solution-state spectrum, contains broader lines at slightly different chemical shifts (Section 3.3).

^{13}C NMR data can be more readily compared between solution and solid than ^{27}Al data, largely because of the influence of the quadrupolar term on the ^{27}Al NMR spectrum, which leads to very broad lines when the aluminium is in an asymmetric environment. In addition, ^{27}Al NMR chemical shifts in the solid state must be corrected for the effect of the second-order quadrupole interaction [34,37]. As a consequence, any comparison of ^{27}Al NMR chemical shifts involving shift differences of a few ppm is fraught with uncertainty. However, gross changes in geometry are readily detected, hence ^{27}Al NMR has been widely used to differentiate between octahedral and tetrahedral aluminium in zeolite chemistry [37,38] owing to the characteristic chemical shifts of these two environments.

2.4. Vibrational spectroscopy

2.4.1. Infrared spectroscopy (IR)

The main use of IR spectroscopy for molecules such as metal complexes is to provide a rapid method for determining that complex formation has indeed occurred,

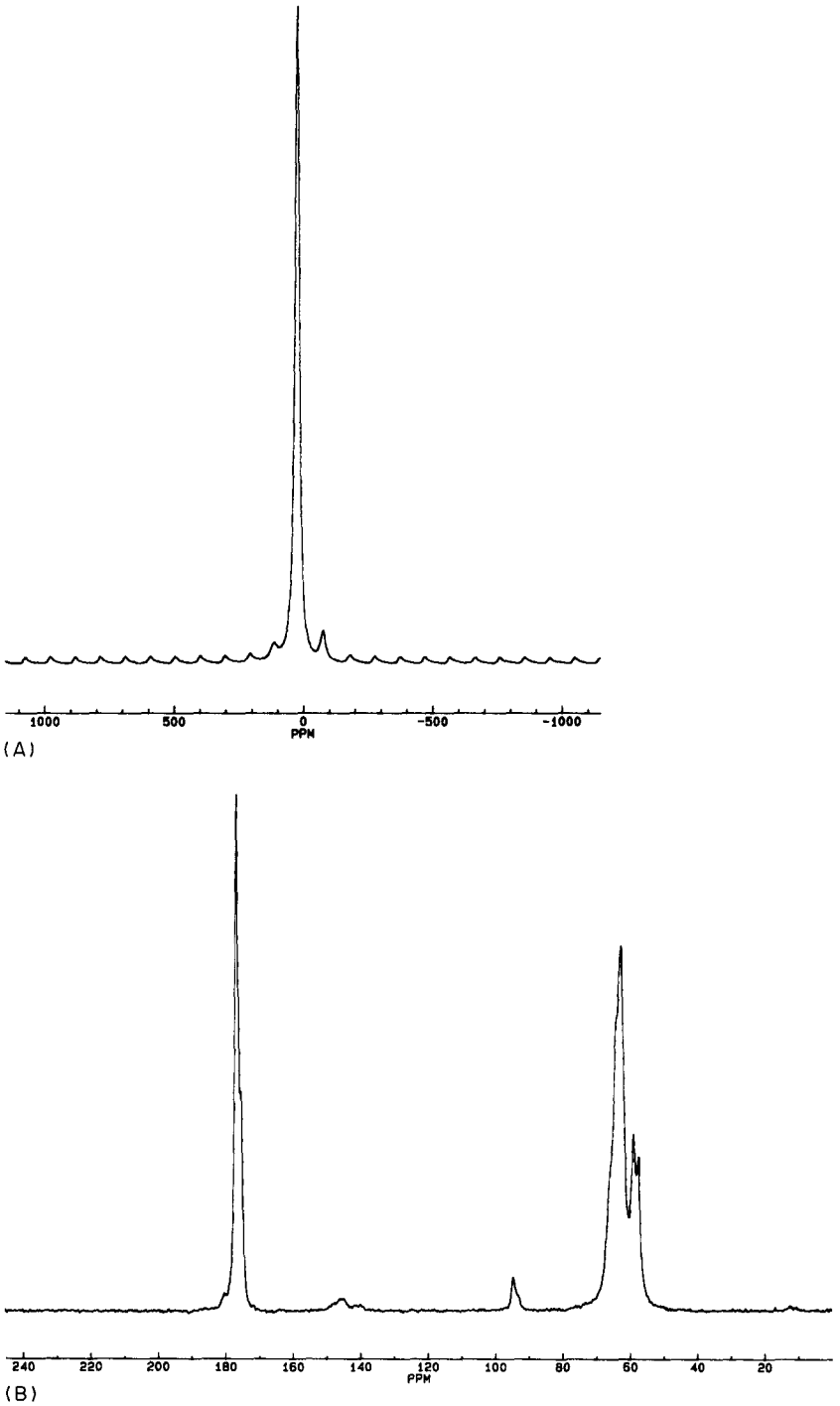

Fig. 8. (A) 52.1 MHz ^{27}Al MAS NMR spectrum of the heidi dimer **1**. Spinning speed, 5020 Hz. 6500 transients were collected using a recycle delay of 0.1 s and a 0.6 μs, $\pi/5$, pulse. (B) 50.32 MHz ^{13}C cross-polarization MAS NMR spectrum of the heidi dimer.

as illustrated by the comparison of IR spectra of free heidi and of heidi bound to Al^{3+} in two different complexes (Fig. 9). Often it is possible to show that the product obtained is different from the starting materials and other complexes, and in some cases specific structural information can be obtained from comparisons with characteristic stretching frequencies of group vibrations, *e.g.* whether or not a carboxylate group has coordinated to a metal ion [40]. The technique is easily applied and does not require single crystals. However, the spectra will be too complicated to allow for a full structural assignment, and often it is not possible to establish whether the sample is pure.

2.4.2. Attenuated total reflectance (ATR)

The study of aqueous solutions of metal–ligand systems by conventional IR spectroscopy is limited by the fact that water absorbs energy in several areas of the IR spectrum, resulting in very strong and broad bands in the regions 3650–2930, 1750–1580 and 930–400 cm^{-1}. To minimize this it is necessary to use solutions of high concentrations in cells with very short optical path lengths, resulting in poor resolution of bands. The method of ATR-IR [41] overcomes these problems and allows an IR spectrum of an aqueous solution of a metal ligand system to be observed, as indicated in Fig. 10.

Fig. 10 shows regions of the ATR-IR spectra of aqueous solutions of heidi and Al^{3+} which yield crystals of heidi bound by Al^{3+} in a dimeric complex, and when bound into an Al_{13} cluster. The bands in the sample spectra were superimposed on the spectrum of water and the water spectrum was subtracted from each sample

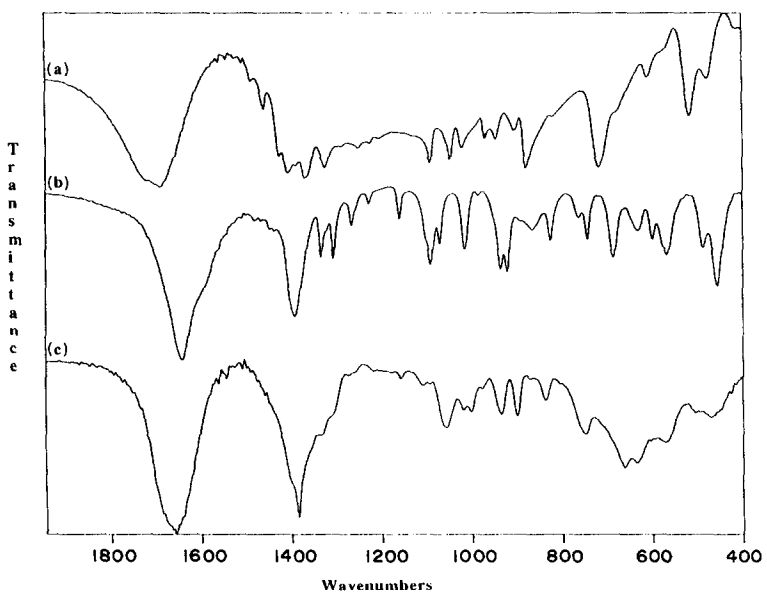

Fig. 9. Comparison of the IR spectra of (a) the free ligand H_2heidi, (b) the complex $[Al(heidi)(H_2O)]_2 \cdot 2H_2O$ (**1**) and (c) the complex $[Al_{13}(\mu_3\text{-}OH)_6(\mu_2\text{-}OH)_{12}(heidi)_6(H_2O)_6]^{3+}$ (**2**).

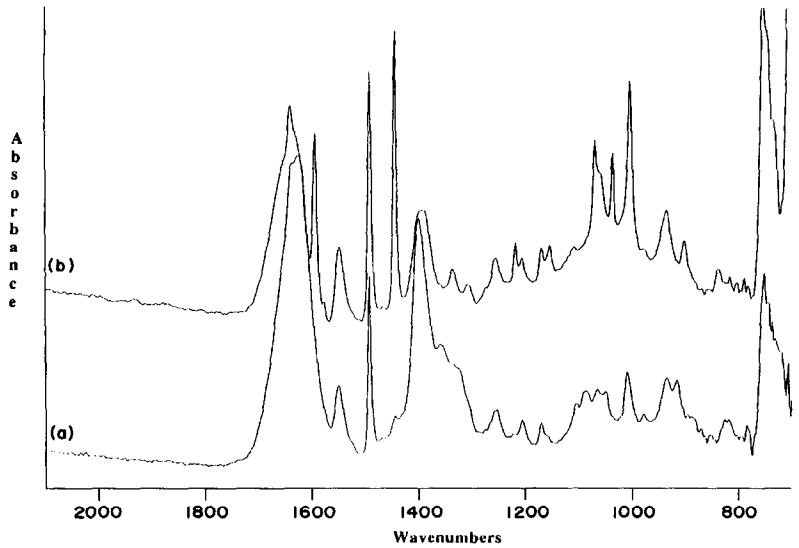

Fig. 10. Comparison of the ATR spectra of (a) 100 mM $AlCl_3$ and 50 mM heidi and (b) 100 mM $AlCl_3$ and 200 mM heidi. Both solutions were adjusted to pH 4.3 with pyridine. Spectra are shown after subtraction of a water background.

spectrum. Clearly the two spectra are different from each other, and they are different from that of free heidi. ATR-IR, like conventional IR, can demonstrate that complex formation has occurred. However, comparison of Fig. 9 with Fig. 10 shows that the corresponding IR and ATR-IR spectra are different. This may be partly because the solutions used for Fig. 10 contain species other than those crystallizing to give the samples used for the IR studies in Fig. 9. However, it is largely because ATR-IR spectra are intrinsically different to comparable IR spectra, hence at the present stage of development vibrational spectroscopy is not capable of detailed structural information to be carried over from solid state to solution.

3. Al^{3+} complexes with the ligand H_2heidi

The ligand H_2heidi, $N(CH_2CO_2H)_2(CH_2CH_2OH)$, has been used extensively in studies of the coordination chemistry of Fe^{3+} [42] and, in part because we are engaged on a comparative study of Fe^{3+} and Al^{3+} complexation chemistry [18], we have chosen heidi to be the main example to illustrate our approach to Al^{3+} speciation.

3.1. Potentiometric studies

Al^{3+}–heidi complexes are the dominant species over the pH range 3–9 at 25 °C in a supporting electrolyte of 0.6 M NaCl, in mixtures of Al^{3+} with heidi at 50 and

5 mM concentrations. Outside this pH range Al^{3+} will be predominantly found as the hexaaquo $[Al(H_2O)_6]^{3+}$ and tetrahydroxo $[Al(OH)_4]^-$ complexes. Equilibrium data were evaluated based on data for the concentration ranges 0.73–3.01 mmol kg^{-1} heidi and 1.43–2.63 mmol $kg^{-1}Al^{3+}$. It was found that experimental equilibrium conditions were rarely achieved in alkaline conditions and hence the data utilized for the calculations were limited to the pH range 2.5–7.0. The major complex species for all systems were the same, $Al_2L(OH)^{3+}$, $Al_2L_2(OH)_2$, $AlL_2(OH)^{2-}$ and $Al_2L_2(OH)_4^{2-}$. The distribution diagram for an aqueous solution of 5 mM Al^{3+} and 5 mM heidi is given in Fig. 11 and the relevant stability constants in Table 1. The distribution profile predicts that the dominant Al–heidi complexes formed will be small monomeric or dimeric aluminium species with one or two heidi ligands. It is expected

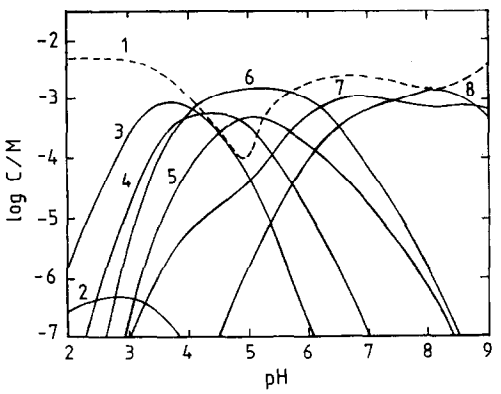

Fig. 11. Distribution diagram of the species for an aqueous solution of 5 mM Al^{3+} + 5 mM heidi: (1) $[Al(III)]_{inorg}$ (sum of $[Al(H_2O)_6^{3+}]$, $[Al(OH)^{2+}]$, $[Al(OH)_2^{+}]$, $[Al(OH)_3]$, $[Al(OH)_4]$, $[Al_3(OH)_4^{5+}]$ and $[Al_{13}(OH)_{32}^{7+}]$); (2) AlL^+; (3) $Al_2L(OH)^{3+}$; (4) $Al_2L(OH)_2^{2+}$; (5) $Al_2L(OH)_3^{+}$; (6) $Al_2L_2(OH)_2$; (7) $AlL_2(OH)^{2-}$; (8) $Al_2L_2(OH)_4^{2-}$. L represents the deprotonated form of the ligand in basic conditions, e.g. heidi $L=L^{2-}=[(CH_2CH_2OH)N(CH_2CO_2^-)_2]^{2-}$. Complexes given as ML represent the solvated form MLX_n (where X = solvent).

Table 1
Stability constant for the complexes of the three-component system Al^{3+}–heidi^{2-}–H^+, according to the formation reaction $mAl^{3+} + l\,L^{2-} + h\,H^+ \rightleftharpoons Al_mL_lH_h^{3m+h-2l}$

m	l	h	Species	Log ($\beta \pm \sigma$)
0	1	2	H_2L	10.745 ± 0.009
1	1	0	AlL^+	7.007 ± 0.065
1	2	−1	AlL_2OH^{2-}	8.148 ± 0.012
2	1	−1	Al_2LOH^{3+}	6.030 ± 0.026
2	1	−2	$Al_2L(OH)_2^{2+}$	1.848 ± 0.016
2	1	−3	$Al_2L(OH)_3^{+}$	−3.041 ± 0.024
2	2	−2	$Al_2L_2(OH)_2$	9.103 ± 0.011
2	2	−4	$Al_2L_2(OH)_4^{2-}$	−3.956 ± 0.080

that the alcohol function of the ligand will be ionized to the alkoxide in all the major complexes with additional ionizations coming from coordinated waters at higher pH.

3.2. X-ray diffraction studies

Various crystallization trials were set up to investigate factors affecting crystal formation. These were run in parallel with NMR investigations, the full details of which have been given previously [18]. During these trials two solid Al–heidi complexes were recovered in a form suitable for structure determination by X-ray diffraction. The dinuclear species $[Al(heidi)(H_2O)]_2 \cdot 2H_2O$ (**1**) was prepared from solutions with an $Al(NO_3)_3$: heidi ratio of 1 : 2 at pH 4.3, and an Al_{13} cluster (**2**) was prepared similarly from solutions with an $Al(NO_3)_3$: heidi ratio of 2 : 1 at pH 5.0. The two aluminium centres in **1** are octahedrally coordinated and bridged by alkoxide arms from two different heidi LH_{-1} ligands (see Fig. 12).

The X-ray structure of **2** again shows the dinucleating function of the alcohol of LH_{-1} heidi. It consists of aluminium clusters in a lattice of hydrogen-bonded nitrate anions and water molecules. The clusters are made up of 13 Al^{3+} ions held together by bridging hydroxide and alkoxide groups (Fig. 13). The cluster core consists of an $[Al_7(\mu_3\text{-}OH)_6(\mu_2\text{-}OH)_6]^{9+}$ unit which, as in the iron analogues [42], corresponds to a portion of a hexagonally close packed hydroxide layer structure with aluminiums in the octahedral holes. These core oxygens all have tetrahedral geometry supporting their assignment as bridging hydroxides. This core is connected to the inside of a shell of six Al–heidi units by μ_2-OH and μ_2-alkoxide bridges from the ligand heidi. The formula of the shell is $[Al_6(\mu_2\text{-}OH)_6(heidi)_6(H_2O)_6]^{6-}$, thus resulting in only three different aluminium environments: the central aluminium, the six aluminiums on the periphery of the core and the six aluminiums in the shell. This is also reflected by the higher crystallographic symmetry of the aluminium cluster compared with the iron analogues.

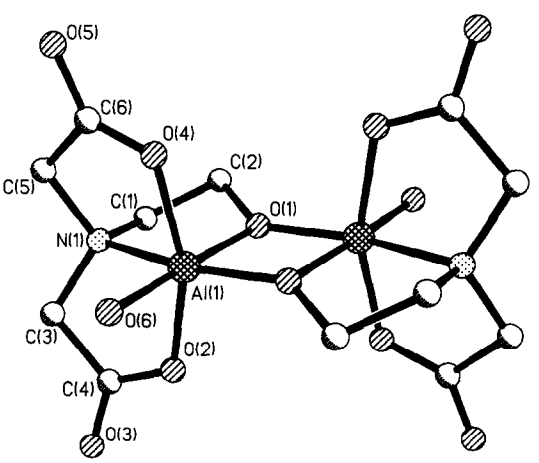

Fig. 12. Structure of $[Al(heidi)(H_2O)]_2 \cdot 2H_2O$ (**1**).

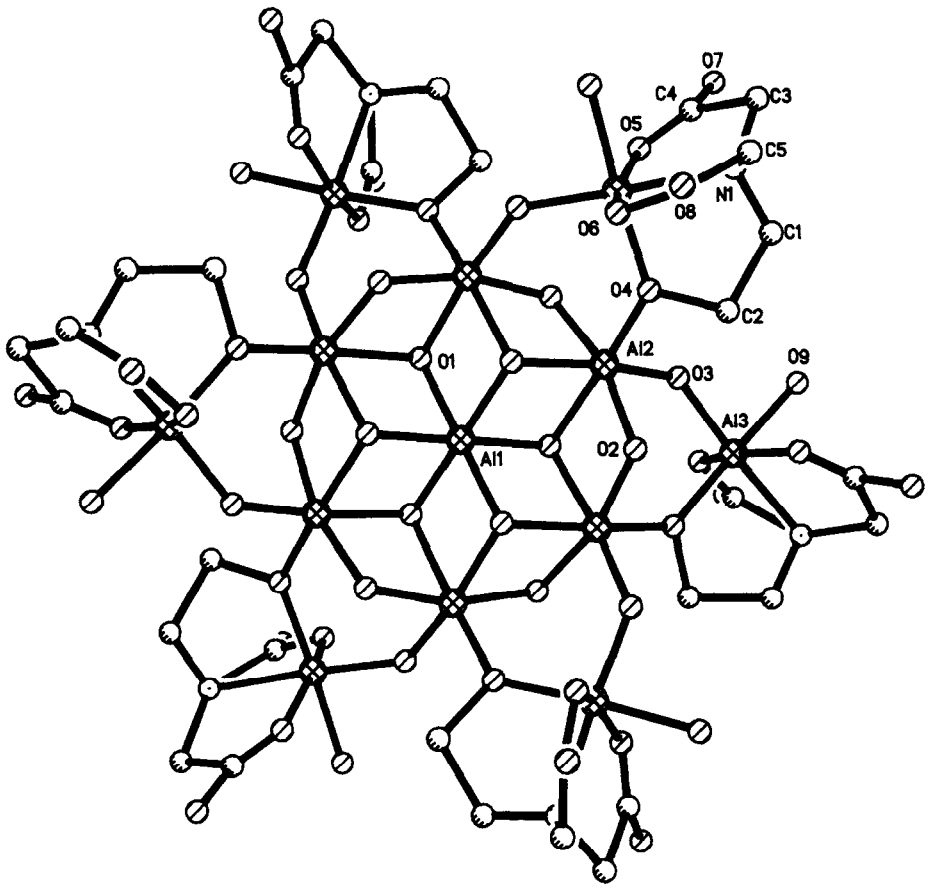

Fig. 13. Structure of $[Al_{13}(\mu_3\text{-}OH)_6(\mu_2\text{-}OH)_{12}(heidi)_6(H_2O)_6]^{3+}$ (2).

In both 1 and 2 the aluminiums are in distorted octahedral environments, which is also evident in the ^{27}Al NMR spectra described below. The previously reported $Na[Al_{13}O_4(OH)_{24}(H_2O)_{12}](SeO_4)_4 \cdot xH_2O$ cluster is different from cluster 2 in that it is a completely inorganic structure with the aluminiums in two different environments, one central tetrahedrally coordinated aluminium with a characteristic NMR signal at 63.5 ppm and twelve octahedrally coordinated metals [33,43,44].

Compound 1 is predicted by the potentiometric studies to be a major component of solutions of Al^{3+}–heidi (Fig. 11) whereas 2 is predicted to be only a minor component at best. Note that we have not crystallized 2 from 1:1 and 1:2 solutions of Al^{3+}–heidi, nor were we able to obtain suitable potentiometric data on the 2:1 solution because of the formation of precipitates. Thus the significance of 2 for the solution speciation of Al^{3+}–heidi is not known. We return to this point below, where it is seen from solution-state NMR studies that the yield of crystallized material is not necessarily representative of the solution speciation.

3.3. Solid-state NMR spectroscopy

Solid-state NMR, in principle, provides an essential link between solution-state NMR and X-ray diffraction studies. However, problems arise in establishing this connection, both for ^{13}C and ^{27}Al NMR, as illustrated by the heidi clusters. Contrasting ^{27}Al magic angle spinning (MAS)NMR spectra were obtained for the two clusters **1** and **2**. In the case of the dimer **1** the ^{27}Al NMR spectrum [Fig. 8(A)] shows a sharp resonance at 22.2 ppm flanked by a series of spinning sidebands separated from the isotropic resonance by the spinning frequency. These sidebands originate from the quadrupolar interaction and their appearance indicates that the ^{27}Al NMR spectrum is determined by the first-order quadrupolar interaction. In contrast, the ^{27}Al MAS NMR spectrum of cluster **2** shows a broad isotropic resonance at 5.8 ppm with no extensive spinning sideband manifold (Fig. 14). Since the material is crystalline, line broadening caused by structural disorder is unlikely. Taken together, these observations suggest that the ^{27}Al NMR spectrum of **2** is dominated by the second-order quadrupolar interaction. One consequence of this is that a straight comparison of the solid-state chemical shift with the solution-state value is not possible. The ^{13}C CPMAS NMR spectra are not much more helpful. That for the dimer **1** [Fig. 8(B)] shows only one broad carbonyl resonance at 176.8 ppm, whereas the solution-state NMR studies described in the following section indicates the dimer has a carbonyl ^{13}C chemical shift of 177.1 ppm. The 0.3 ppm shift between solid and solution states is less than the solid-state resonance linewidth, and it could arise from a number of causes (Section 2.3.3). Since a monomeric species has a solution state carbonyl ^{13}C chemical shift of 176.8 ppm, it is clear that this approach does not assist in determining whether the solid complex persists in solution. The similarity in ^{27}Al NMR chemical shift of the dimer is, however, more encouraging.

3.4. Solution-state NMR spectroscopy

Solution-state NMR plays a key role in defining the speciation of the Al–heidi system. Aspects investigated include optimization of the crystallization conditions, investigation of the stability of solid structures on being redissolved and correlation of potentiometric distribution profiles with structural and spectroscopic parameters. Examples of each of these are given below. Note that the 1D ^{1}H NMR spectrum of heidi is not particularly informative, so our studies were concentrated on ^{27}Al and ^{13}C NMR. The carbonyl region is the main area of interest in the ^{13}C spectra, with a clear distinction seen between the signals from the free ligand and those signals from the ligand complexed to Al^{3+}.

3.4.1. Crystallization solution

The ^{27}Al NMR spectrum of the crystallization solution for the dinuclear cluster **1** has features at 0 ppm, arising from $[Al(H_2O)_6]^{3+}$, and at 25 ppm, which we assign to **1** [Fig. 15(A)]. The spectrum of the crystallization solution for the Al_{13} cluster **2** [Fig. 15(B)] has a signal at 2 ppm, which probably comes from a dimeric hydroxo bridged species [33], the 25 ppm signal assigned to the dinuclear species **1** and a

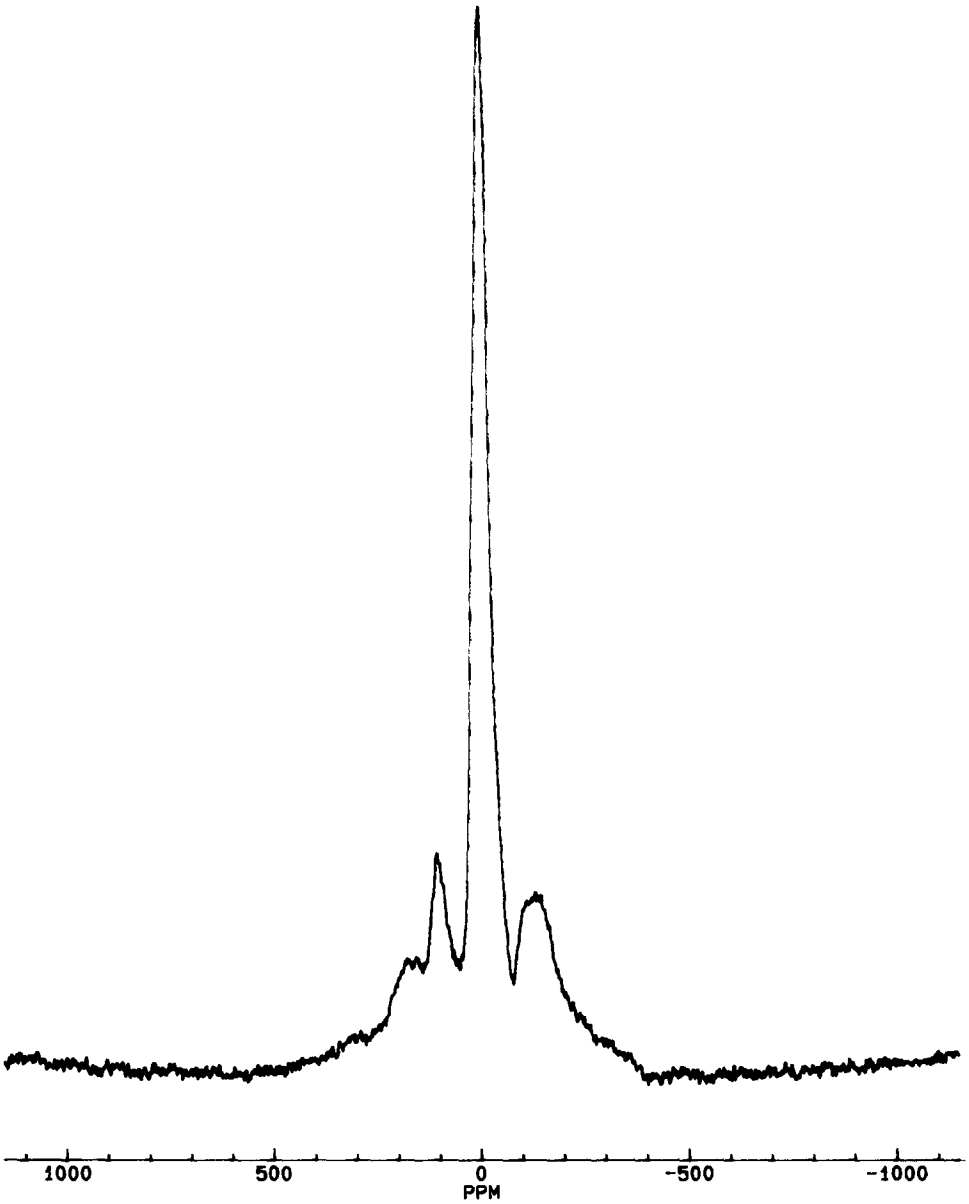

Fig. 14. 52.1 MHz ^{27}Al MAS NMR spectrum of the heidi cluster **2**. Spinning speed, 5010 Hz. 2500 transients were collected using a recycle delay of 0.1 s and 0.6 μs, $\pi/5$, pulse.

broad underlying signal at 20 ppm, which probably arises from the Al_{13} cluster **2** (see Section 3.3). The absence of a peak at 0 ppm from $[Al(H_2O)_6]^{3+}$ indicates that the solution conditions in Fig. 15(B) are the optimum conditions for isolating high

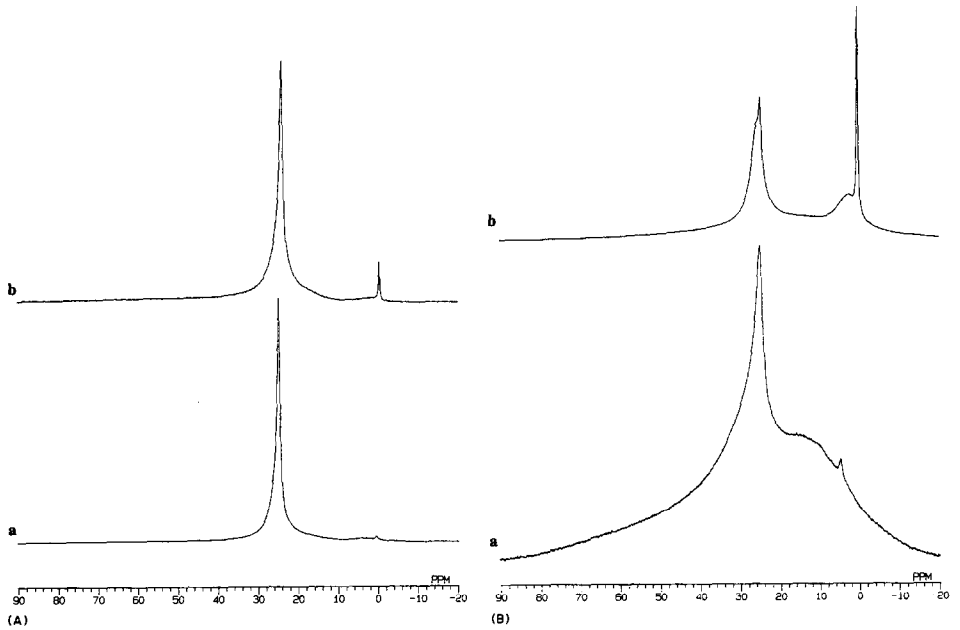

Fig. 15. 104.5 MHz ^{27}Al NMR spectra of the crystallization solutions of (A) **1** ([Al] = 0.125 M, [heidi] = 0.25 M, pH = 4.3) and (B) **2** ([Al] = 0.25 M, [heidi] = 0.125 M, pH = 5.0): (a) before crystal formation; (b) after crystal formation. There is little change in the signals before and after crystallization of **1**, with the large decrease in intensity of the signal at 25 ppm, shown by the relative increase in the $[Al(H_2O)_6]^{3+}$ signal, consistent with the assignment of this peak to the dimer **1**. Under conditions known to yield **2** there is a marked decrease in intensity of the broad signal at 20 ppm after the formation of crystals, consistent with its assignment to the solid species formed.

yields of the Al_{13} cluster. Note that the concentration of these solutions was much greater than that used for subsequent NMR experiments, since the initial aim was to crystallise and characterize single species.

3.4.2. Solutions of crystals

NMR studies of solutions of crystals of **1** and **2** in water showed that both redissolved structures are stable with time. After a slight initial change indicating some formation of the dimer **1**, there is no further change in the ^{27}Al NMR spectrum of **2** over a period of 4 weeks (Fig. 16). The spectrum of **1** redissolved in water is slightly different from that seen in the solid state, with a shoulder appearing at high frequency of the signal from **1**, at 25 ppm. This arises from partial hydrolysis of **1** accompanying the physical destruction of the crystals to aid solubilization. As with the spectrum from **2**, the spectrum of **1** remains stable over a period of 4 weeks. The ^{13}C NMR of the redissolved dimer **1** confirms that partial hydrolysis occurs with signals from both monomeric and dimeric complexes seen. A solution of the redissolved cluster **2** has a carbonyl resonance at 177.8 ppm. This occurs just to low field of the 1 : 1 monomer and can be observed in crystallization solutions.

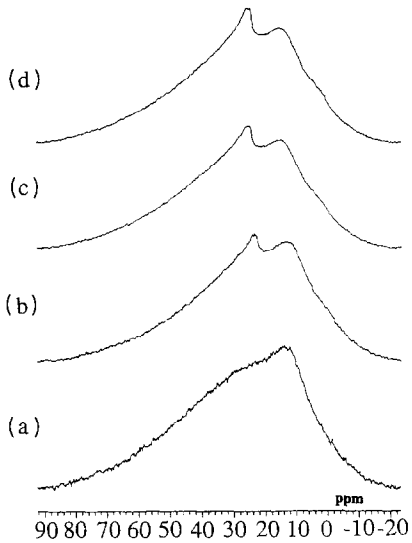

Fig. 16. 104.5 MHz ^{27}Al NMR spectra of crystals of the Al_{13} cluster **2** dissolved in D_2O at the following times after dissolution to give an Al^{3+} concentration of approximately 20 mM: (a) 5 min; (b) 5 h; (c) 14 h; (d) 72 h.

^{27}Al NMR shows that the redissolved cluster **2** is less stable to changes in temperature with the appearance of a sharp dimer peak at 25 ppm seen as the temperature is increased from 25 to 60 °C (Fig. 17(B)). The corresponding temperature profile for the dimer **1** in solution shows no new signals appearing above 25 °C, although the decrease in peak width with elevated temperature allows a better resolution of the lowfield shoulder to the signal at 25 ppm (Fig. 17(A)). The apparent stability of the redissolved crystals is reversed on increasing the pH of the solutions from an autogeneous value of about pH 4.3. The solution of the dimer shows a decrease in intensity of the 25 ppm signal accompanied by the appearance of a number of broad features which correspond exactly to the spectral changes observed for the pH titration of a 1:2 Al:heidi solution (see later). The ^{27}Al NMR spectrum of a solution of redissolved **2** is apparently unchanged immediately after alteration of its pH to 7, but after 2 weeks the spectrum is very similar to that of the redissolved dimer at pH 7. The compositions of the two solutions are not identical owing to the reduced amount of ligand present in **2**; this is reflected in the magnitude of the broad features seen in the spectrum from **2**. This may be because, although at pH 7 **1** is more stable than **2**, the rates of exchange between them are very slow. Given that the rates of ligand exchange are slow for these complexes, it is hard to determine whether the solid species obtained are a result of kinetic or thermodynamic factors. The temperature instability and slow rate of change in the pH titration of the solution of **2** indicates that kinetic factors may play an important part in crystallization whereas the temperature stability and fast change with pH for **1** in solution may indicate that this is the thermodynamically favoured species for the conditions employed.

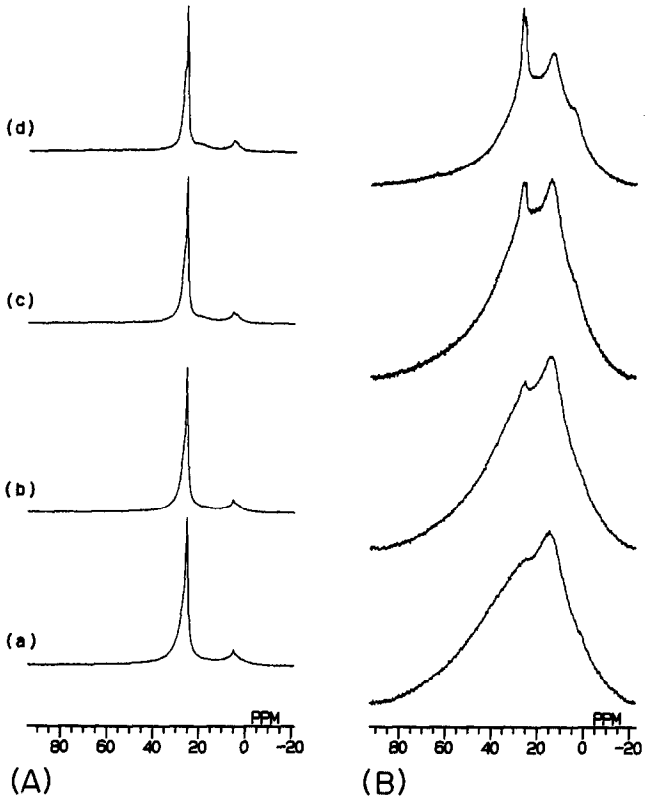

Fig. 17. 104.5 MHz ^{27}Al NMR spectra showing the affect of temperature on redissolved crystals of **1** and **2** (**A**) 30 mM **1**, pH 4.3: (a) 25: (b) 37; (c) 50; (d) 65 °C. (**B**) 20 mM **2**, pH 4.5: (a) 25; (b) 37; (c) 50; (d) 65 °C.

3.4.3. Speciation of aluminium under conditions parallel to the potentiometric studies

In order to follow the speciation of aluminium under conditions parallel to the potentiometric studies (analytical concentration ca. 50 mM), freshly prepared solutions of $Al(NO_3)_3 \cdot 9H_2O$ in D_2O adjusted to pH 4 with NaOD and containing variable amounts of heidi in the Al:heidi molar ratio range 1:0–1:2 were studied by ^{27}Al NMR (Fig. 18). In the absence of heidi, peaks at 0 ppm, arising from $[Al(H_2O)_6]^{3+}$, and at 63.5 ppm, arising from the tetrahedrally coordinated aluminiums of $[Al_{13}O_4(OH)_{24}(H_2O)_{12}]^{7+}$ [31], were observed. In the presence of heidi three other signals were present with chemical shifts of 26, 25 and 2 ppm. The broad signal at 2 ppm, assigned to a dimeric hydroxo-bridged species, remained even at high heidi concentrations, but the intensities of the two signals at 25 and 26 ppm increased with increasing heidi concentration. The peak at 25 ppm can be assigned to the dinuclear species **1** as above, although the state of the compound may be $Al_2L_2(OH)_2$, which is predicted to be the major species by potentiometric measurements, as opposed to the neutral $Al_2L_2(H_2O)_2$. The broader signal at 26 ppm is probably attributable to an $Al_2L(OH)_n$ species. At all Al^{3+}:heidi ratios studied,

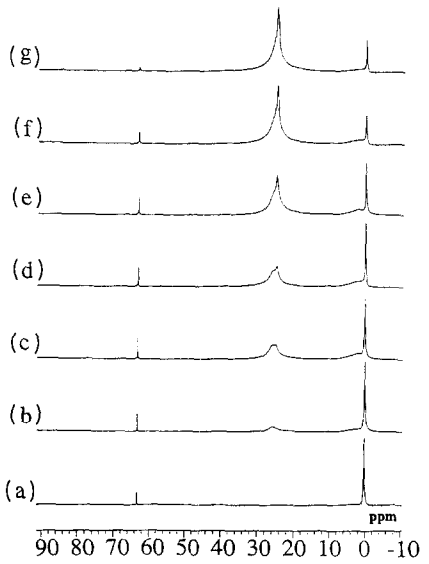

Fig. 18. 104.5 MHz ^{27}Al NMR spectra of $Al(NO_3)_3$ and heidi in D_2O. Addition of heidi to 50 mM Al^{3+} at pH 4.0; [heidi] = (a) 0; (b) 10; (c) 20; (d) 25; (e) 33; (f) 50; (g) 100 mM.

signals from $[Al_{13}O_4(OH)_{24}(H_2O)_{12}]^{7+}$ and $[Al(H_2O)_6]^{3+}$ were observed, although at higher ligand concentrations these are only present as minor species. However, in none of these spectra were signals clearly arising from the Al_{13} cluster **2** observed. This is probably a result of the relatively low symmetry of the aluminium centres, which give rise to broad peaks (Fig. 16), and because the yield of crystallized material is not necessarily representative of the percentage of the species in solution. In support of this latter point, the ^{27}Al NMR data at various pH values (Fig. 19) indicate the presence of at least five different aluminium-containing species in solution and, as expected at these low aluminium concentrations, some of these are Al^{3+}–hydroxo species. These results are in broad agreement with the potentiometric data (Fig. 11) with regard to the major species present, but with ^{27}Al NMR it is not possible to observe signals from all the minor species that are predicted, largely owing to overlap of low-intensity signals with signals from more abundant species, but also the possibility that they might not be resolved from the underlying probe background.

In order to resolve minor species from the major species, ^{1}H and ^{13}C NMR spectroscopy were used. The ^{13}C and corresponding ^{27}Al NMR spectra for a range of Al–heidi solutions are shown in Fig. 20. The ^{13}C NMR spectra all show at least five signals from Al–heidi complexes, indicating the presence of a number of minor species in solution in addition to the major species previously identified. However, owing to the complexity of these signals it was not possible to assign species firmly to individual resonances, although it was possible to group ^{13}C signals into different forms of Al–heidi complexes. The signals centred at 177.6 ppm are from the Al–heidi 1 : 1 complexes, and to high field of these are the signals based on the dimer **1** centred

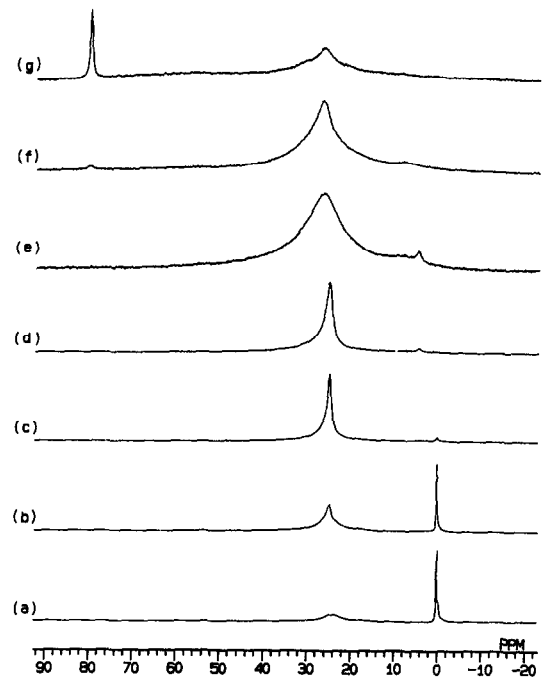
(g)
(f)
(e)
(d)
(c)
(b)
(a)
PPM
90 80 70 60 50 40 30 20 10 0 -10 -20

(A)

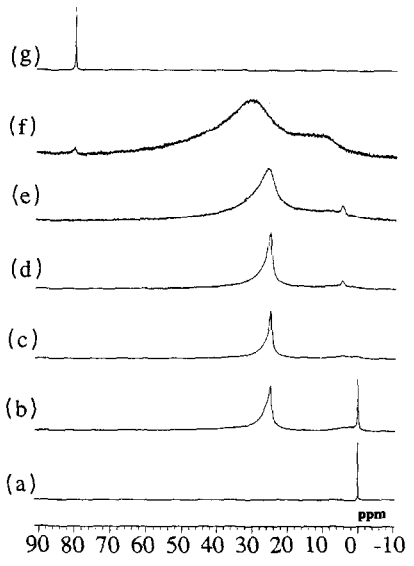
(g)
(f)
(e)
(d)
(c)
(b)
(a)
ppm
90 80 70 60 50 40 30 20 10 0 -10

(B)

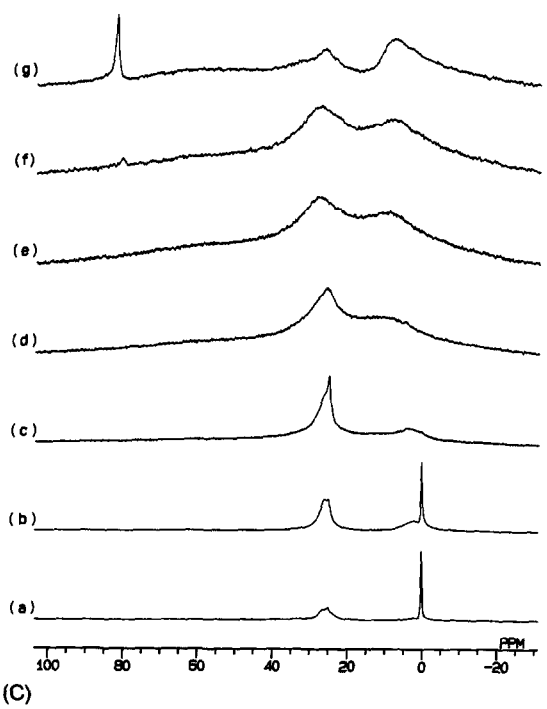
(g)
(f)
(e)
(d)
(c)
(b)
(a)
PPM
100 80 60 40 20 0 -20

(C)

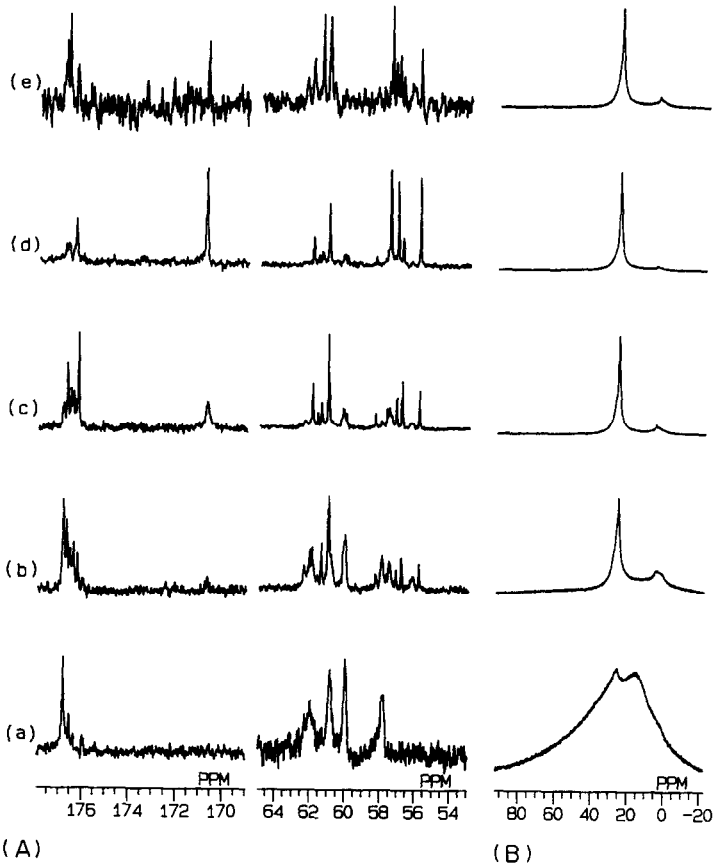

Fig. 20. (A) 101 MHz ^{13}C NMR and (*B*) 104 MHz ^{27}Al NMR spectra of Al^{3+} and heidi: (a) 30 mM redissolved **2**, pH 4.3; (b) 100 mM Al^{3+} + 50 mM heidi, pH 4.7; (c) 100 mM Al^{3+} + 100 mM heidi, pH 4.8; (d) 100 mM Al^{3+} + 200 mM heidi, pH 4.8; (e) 20 mM redissolved **1**, pH 4.5.

at 177.1 ppm. The different signals observed for each form of Al^{3+}–heidi complex probably reflect different states of hydrolysis, i.e. $Al_2L(OH)^{3+}$, $Al_2L_2(OH)_2$, $AlL_2(OH)^{2-}$ and $Al_2L_2(OH)_4^{2-}$, as predicted by the potentiometric studies.

Analysis of the 1D ^1H NMR spectra is hindered by the large number of signals observed (three from each complex), leading to a very broad feature at 3.6 ppm coming from many overlapping resonances where no clear assignments can be made. To resolve some of the features 2D ^1H–^1H COSY spectra were acquired for Al : heidi 2 : 1, 1 : 1 and 1 : 2 solutions at pH 4.8. Analysis of the cross peaks shows the presence

Fig. 19. 104.5 MHz ^{27}Al NMR spectra of $Al(NO_3)_3$ and heidi in D_2O. pH titration of (A) 100 mM Al^{3+} and 200 mM heidi at: pH (a) 2.80, (b) 3.14, (c) 3.88, (d) 5.16, (e) 6.38, (f) 8.95 and (g) 9.7; (B) 100 mM Al^{3+} and 100 mM heidi at pH (a) 2.47, (b) 3.62, (c) 4.17, (d) 5.01, (e) 6.00, (f) 8.67 and (g) 10.47; (C) 100 mM Al^{3+} and 50 mM heidi at pH (a) 3.11, (b) 3.82, (c) 4.57, (d) 5.83, (e) 7.30, (f) 8.41 and (g) 9.49.

of at least six heidi species in each solution; Fig. 21 illustrates this for the 1:2 solution. It is possible to assign cross peaks to the major 2:2 dimeric and 2:1 monomeric Al^{3+}–heidi species, but without quantitative analysis it is not possible to assign further signals.

The speciation is strongly pH dependent, as indicated by Fig. 11 and supported by the ^{27}Al NMR spectra in Fig. 19. In general, the NMR studies parallel the potentiometric studies well. pH titrations were performed with 2:1, 1:1 and 1:2 solutions of Al–heidi with the addition of base being monitored by NMR. All showed the progression of aluminium from the free $[Al(H_2O)_6]^{3+}$ species through different Al–heidi complexes to the free $[Al(OH)_4]^-$ species, and all follow a similar pattern sharing a number of common signals, the stability of which is dependent on the solution composition and pH. The simplest system is the Al^{3+}–heidi 1:2 solution, which is dominated by a single signal for much of the titration. There is evidence for complex formation above pH 2.0 with two signals at 25.0 and 24.2 ppm clearly seen at pH 2.8. The narrower high-frequency signal is from the dimer **1** as outlined earlier, while the signal just to lower frequency is probably from the $\{Al(heidi)(H_2O)_3\}^+$ species, in which heidi acts as a tridentate ligand and the formation of alkoxide is suppressed by the low pH. On further addition of base the

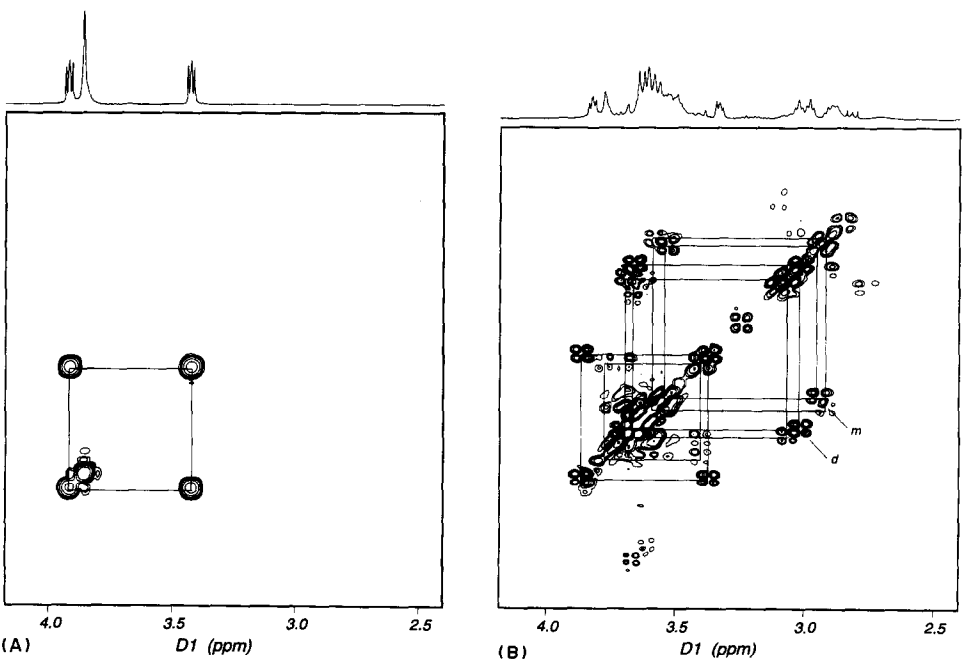

Fig. 21. 400 MHz ^1H NMR spectra of $Al(NO_3)_3$ and heidi in D_2O. (**A**) 2D-COSY of 0.05 M heidi at pH 4.8; (**B**) 2D-DQF COSY of 0.1 M Al^{3+} + 0.05 M heidi at pH 4.8. Each box represents a different heidi species. Thus, for the free ligand there is one species but in the presence of Al^{3+} six types of heidi can be resolved, with *m* and *d* representing the major 2:1 monomeric and 2:2 dimeric Al^{3+}–heidi complexes, respectively.

signal from **1** is seen to increase as more Al^{3+} becomes complexed. This strong signal dominates the 25 ppm region of the spectrum, making it hard to monitor any minor species present. However, there is a change between pH 3.0, showing a shoulder to low frequency, and pH 3.5, where a high-frequency shoulder is observed. This is likely to indicate a change in the minor species from a tridentate heidi–Al^{3+} complex to a tetradentate heidi–Al^{3+} complex following deprotonation of the second carboxylate function, which will be favoured with increasing pH, allowing a maximum chelate effect. At pH 4.1 complete complexation of Al^{3+} has occurred with the dominant species being the dimer **1**, which remains up to pH 8.5. The broadening effect seen above pH 5.5 can be attributed to a combination of hydrolysis of **1** to the $\{Al_2L_2(OH)_3\}^-$ and $\{Al_2L_2(OH)_4\}^{2-}$ complexes and a reorganization in solvation by the outer-shell waters. Two other signals are clearly seen during the titration and the broad signals obtained around pH 7.0 could mask the presence of others. Above pH 4.5 a new signal is seen at 6.3 ppm which increases in intensity up to pH 7.0, where it becomes masked by another new signal centred at 10 ppm. The narrow linewidth and high field position of the 6.3 ppm signal indicates that it is from a small monomeric or dimeric complex that is only complexed to oxygens (Fig. 7). This signal is not observed for the hydrolysis of Al^{3+} in the absence of chelating ligands [33], suggesting that it is from an Al^{3+}–heidi complex. The broad signal at 10 ppm is a clear indication of an unsymmetric, and probably polymeric, Al^{3+} species. Above pH 8.0 a new signal appears at 80 ppm from $[Al(OH)_4]^-$. Further additions of base see the complete conversion of the other forms of Al^{3+} to $Al(OH)_4^-$, which is the only species observed at pH 10.0.

The pH titration of the Al–heidi 1:1 system follows very similar lines. Complex formation is seen above pH 2.0 with initial formation of three complexes. Further hydrolysis establishes the dimer as the major species. The weak signal that appears at 2 ppm above pH 3.5 is from the inorganic hydroxo-bridged aluminium dimer. Increasing the pH from 4.0 to 5.5 shows little difference to the Al–heidi 1:2 system, with the signal at 25.5 ppm broadening and the growth of the signal at 6.3 ppm. The appearance of the broad features previously seen occurs at lower pH than before, leading to a loss in resolution and sensitivity, and increases up to pH 8.5 where the formation of $[Al(OH)_4]^-$ becomes favoured over further complex formation. This behaviour is consistent with these broad features being attributable to higher nuclearity clusters which can be formed more readily when reduced amounts of ligand are present.

Titration of the Al–heidi 2:1 system fits a predictable pattern. Complex formation is seen above pH 2.0 with signals from two major and one minor complex at ca 25.6, 25.0 and ca 24.2 ppm. The appearance of broad features is seen at a lower pH than for the equivalent Al–heidi 1:1 system and these dominate the spectrum above pH 6.5. Given the poor resolution of these broad features it is not possible to assign signals definitely to complexes, but the spectrum seen at pH 5.8 contains a number of similarities to those obtained from solutions of **2**. This may indicate that formation of **2** can occur readily in hydrolysed solutions of Al^{3+} when there are reduced amounts of ligand present at low concentrations ($[Al] = 100$ mM). At pH 7.0 the spectrum is similar to those seen in the other systems with two signals at 28 and

18 ppm overlaid on a broad background. Formation of $[Al(OH)_4]^-$ is seen above pH 8.0.

4. Conclusion

The solution-state NMR and potentiometric studies are in reasonable agreement concerning the number and identity of the major Al^{3+}–heidi components present. What is uncertain is the exact structures of these major species. Crystals have been obtained from a dimeric species and from an Al_{13} cluster, but only the former may represent a thermodynamically preferred form in solution. The use of solid-state ^{27}Al NMR to bridge the gap between the solution-state NMR and crystal studies appears to be effective in the case of the symmetric dimer but is problematic for the cluster, but solid-state ^{13}C NMR was not helpful, and nor was comparative solution- and solid-state vibrational spectroscopy. Further progress on determining the solution speciation of the Al^{3+}–heidi system requires crystallization of other Al^{3+}–heidi species that are components of the solutions.

Acknowledgements

We thank the Wellcome Trust for supporting our work through the award of a Toxicology Studentship to P.A.J., the BBSRC/EPSRC for their support of the UEA Centre for Metalloprotein Spectroscopy and Biology and the European Science Foundation for the award of a fellowship to A.T.

References

[1] H. Sigel and A. Sigel (Eds.), Metal Ions in Biological Systems, Vol. 24: Aluminium and its Role in Biology, Marcel Dekker, New York, 1988.
[2] M. Nicolini, P.F. Zatta and B. Corain (Eds.), Aluminium in Chemistry, Biology and Medicine, Cortina International, Verona, 1991.
[3] D.F. Chadwick and J. Whelan (Eds.), Aluminium in Biology and Medicine, Ciba Foundation Symposium No. 169, Wiley-Interscience, Chichester, 1992.
[4] D.P. Perl, in (H. Sigel and A. Sigel (Eds.), Metal Ions in Biological Systems, Vol. 24: Aluminium and its role in Biology, Marcel Dekker, New York, 1988, pp. 259–283.
[5] D.N.S. Kerr, M.K. Ward, H.A. Ellis, W. Simpson and I.S. Parkinson, in D.F. Chadwick and J. Whelan (Eds.), Aluminium in Biology and Medicine, CIBA Foundation Symposium No. 169 Wiley-Interscience, Chichester, 1992, pp. 123–141.
[6] F. Pearce (ed.), Acid Rain, Penguin, Hormandsworth, 1987.
[7] C.T. Driscoll, Jr., J.P. Baker, J.J. Bisogni, Jr., and C.L. Schofield, Nature (London), 284 (1980) 161.
[8] R.B. Martin, Acc. Chem. Res., 27 (1994) 204.
[9] A.L. Crumbliss and J.M. Garrison, Comments Inorg. Chem., 8 (1988) 1.
[10] J.H. Brock, in P.M. Harrison, (Ed.), Metalloproteins: Part 2, Macmillan, Basingstoke, 1985, pp. 183–262.
[11] E.N. Baker and P.F. Lindley, J. Inorg. Biochem., 47 (1992) 147.

[12] R.R. Crichton and R.J. Ward, in R.B. Lauffer (Ed.), Iron and Human Disease, CRC Press, Boca Raton, FL, 1992, p. 23.
[13] P. Aisen and I. Listowsky, Annu. Rev. Biochem., 49 (1980) 357.
[14] G.R. Moore, in Encyclopaedia of Inorganic Chemistry, Wiley, Chichester, in press.
[15] E.C. Theil, Adv. Enzymol, 63 (1991) 421.
[16] P.M. Harrison, S.C. Andrews, P.J. Artymiuk, G.C. Ford, J.R. Guest, J. Hirsmann, D.M. Lawson, J.C. Livingstone, J.M.A. Smith, A. Treffry and S.J. Yewdall, Adv. Inorg. Chem., 36 (1991) 449.
[17] J.D. Birchall and J.S. Chappell, Lancet (1988) 1008.
[18] S.L. Heath, P.A. Jordan, M. Helliwell, G.R. Moore and A.K. Powell, J. Inorg. Biochem., in press.
[19] A. Tapparo, S.L. Heath, P.A. Jordan, G.R. Moore and A.K. Powell, J. Chem. Soc., Dalton Trans., in press.
[20] C.F. Baes and R.E. Mesmer (Eds.), The Hydrolysis of Cations, Wiley-Interscience, New York, 1976.
[21] M. Meloun, J. Havel and E. Högfeldt (Eds.), Computation of Solution Equilibria: a Guide to Methods in Potentiometry, Extraction, and Spectrophotometry, Ellis Horwood, Chichester, 1988.
[22] A.E. Martell and R.J. Motekaitis (Eds.), Determination and Use of Stability Constants, VCH, New York, 1988.
[23] L.O. Öhman and S. Sjöberg, Coord. Chem. Rev., 149 (1996) 33.
[24] A. Sabatini, A. Vacca and P. Gans, Coord. Chem. Rev., 120 (1992) 389.
[25] P. Aisen, A. Leibman and J. Zweier, J. Biol. Chem., 253 (1978) 1930.
[26] A.E. Martell, R.J. Motekaitis and R.M. Smith, Polyhedron, 9 (1990) 171.
[27] L.O. Öhman and S. Sjöberg, J. Chem. Soc., Dalton Trans., (1983) 2513.
[28] L.O. Öhman, Inorg. Chem., 27 (1988) 2656.
[29] C.T. Driscoll and R.D. Letterman, J. Environ. Eng., 114 (1988) 21.
[30] G.E. Jackson, Polyhedron, 9 (1990) 163.
[31] D.J. Clevette, Polyhedron, 9 (1990) 151.
[32] A.K. Powell and S.L. Heath, Coord. Chem. Rev., 149 (1996) 59.
[33] J.W. Akitt, Prog. Nucl. Magn. Reson. Spectrosc., 21 (1989) 1.
[34] J.J. Delpuech, in P. Laszlo (Ed.), NMR of Newly Accessible Nuclei, Vol. 2: Chemically and Biochemically Important Elements, Academic Press, London, 1983, pp. 153–196.
[35] R.K. Iyer, S.B. Karweer and V.K. Jain, Magn. Reson. Chem., 27 (1989) 328.
[36] S.J.A. Fatemi, D.R. Williams and G.R. Moore, J. Inorg. Biochem., 46 (1991) 35.
[37] C.A. Fyfe (Ed.), Solid State NMR for Chemists, CFC Press, Ontario, 1983.
[38] G. Engelhardt and D. Michel (Eds.), High-Resolution Solid-State NMR of Silicates and Zeolites, J Wiley, Chichester, 1987.
[39] P.A. Jordan, N.J. Clayden, G.R. Moore and A.K. Powell, J. Chem. Soc., Chem. Commun., to be submitted.
[40] E.A.V. Ebsworth, D.W.H. Rankin and S. Craddock (Eds.), Structural Methods in Inorganic Chemistry, Blackwell, Oxford, 1987.
[41] C.N. Banwell, Fundamentals of Molecular Spectroscopy, McGraw-Hill, New York, 1983, p. 113.
[42] S.L. Heath and A.K. Powell, Angew. Chem., Int. Ed. Engl., 31 (1992) 191.
[43] G. Johansson, Acta Chem. Scand., 14 (1960) 771.
[44] G. Johansson, Ark. Kemi, 20 (1963) 305.